# GAS ENTRAINMENT PHENOMENON INSIDE AN INVERTED-SHROUD GAS SEPARATOR

**Marcel Cavallini Barbosa, marcelcavbar@gmail.com**
**Luis Enrique Ortiz-Vidal, leortiz@sc.usp.br**
University of Sao Paulo (USP), Sao Carlos School of Engineering (EESC), Mechanical Engineering Department, Av. Trabalhador Sao-Carlense, 400, Sao Carlos, 13566-590, Brazil

**Valdir Estevam**
PETROBRAS, E&P-ENGP/IPP/EE, Av. Rep. Chile, 330, 7º, Centro, Rio de Janeiro, 20031-170, Brazil

**Ricardo Soares Minette**
PETROBRAS, CENPES-PDEP/TEE, Cidade Universitária, Ilha do Fundão, Rio de Janeiro, 21949-900, Brazil

**Oscar Mauricio Hernandez Rodriguez, oscarmhr@sc.usp.br**
University of Sao Paulo (USP), Sao Carlos School of Engineering (EESC), Mechanical Engineering Department, Av. Trabalhador Sao-Carlense, 400, Sao Carlos, 13566-590, Brazil

***Abstract.*** *The Inverted-Shroud (IS) separator is a promising solution for gas-liquid separation in the oil and gas industry. The IS separator combines high gas separation efficiency with the inexistence of moving mechanical parts. It consists of a closed-end tube (shroud) located between the production pipe (tubing) and the well casing. Experimental studies on the IS separator suggest that gas separation efficiency is affected by air entrainment inside the apparatus, where liquid in a free-surface flow impacts the internal liquid surface and carries with it gas that is entrained and disperses into bubbles due to turbulent kinetic energy dissipation. According to phenomenological models from the literature, the prediction of the energy dissipation rate correlates with the entrained bubble size, among other factors. The purpose of this paper is to study the gas entrainment phenomenon on the IS separator. First, a review of the current state-of-the-art research for a similar geometry is presented. Then, a comparison between experimental bubble size and predictions is performed. Bubble size distributions were obtained with a 3-D Optical Reflectance Measurement (ORM) probe installed in an experimental IS-separator test section. Different methods of average diameter (Sauter, mean, median and maximum size) are used to determine which best adjusts to the models' predictions. Results will improve the understanding of the IS separator and make possible the enhancement of its current modeling.*
***Keywords****: Air entrainment, gas-liquid separation, plunging liquid jet, bubble size, inverted-shroud*

## 1. NOMENCLATURE

| | |
|---|---|
| *d* | Particle diameter |
| *E* | Energy dissipation rate |
| *L* | Length |
| *Q* | Velocity |

**Greek characters**

| | |
|---|---|
| $\sigma$ | Superficial tension |
| $\rho$ | Specific mass |

**Subscripts**

| | |
|---|---|
| *average* | Simple arithmetic average |
| *Dis* | Energy dissipation |
| *fs* | Free-surface flow |
| *IAL* | Inner Annular Level |
| *max* | Size larger than 99% of the particles in a given distribution |
| *probe* | Probe window |
| *Sauter* | Sauter average |
| *w* | Water |

## 2. INTRODUCTION

In oil extraction operations that use centrifugal submersed pumps, the presence of free gas can be a source of cavitation problems, especially when for example the gas forms a Taylor bubble prior to reaching the suction of the pump. Countermeasures must be taken by the oil industry to avoid this issue, usually involving the development and installation of an apparatus upstream of the pump that can direct the bubbles elsewhere through flotation or centrifugal force. Failure to adequately separate the free gas before it reaches the suction of the pump can result in high maintenance costs and a loss of production days. Recent studies at the Thermal-fluids Engineering Laboratory of the University of Sao Paulo at Sao Carlos campus (LETeF-EESC-USP) show the Inverted-Shroud (IS) separator can be a solution for separating the free gas before the suction of the pump. The IS separator presents high gas separation efficiency and absence of moving mechanical parts (Ortiz-Vidal (2010), Ortiz-Vidal et al. (2012), Mendes (2012) and Barbosa (2015)). The researches have shown that the efficiency of gas separation is a function of the gas entrainment process inside of the IS separator, more specifically of the penetration depth of the bubbles generated at the impact

between the free-surface liquid flow and the internal liquid surface inside the IS-separator (Ortiz-Vidal et. al (2012)). The better the understanding of gas entrainment process, the greater the improvements of the IS-separator's performance.

Gas entrainment is a phenomenon believed to occur when the impact velocity of the jet exceeds a critical value, when gravitational forces (pressure) overcome surface tension. This mechanical penetration of gas in a liquid phase is commonly observed in practice, in a wide range of environmental situations and industrial applications. In addition to the IS separator, this phenomenon occurs, for example, in spillways (self-aeration), open channels and pipe bends, along with aeration in bubble column reactors and pump intakes and gas entrainment from plunging liquid jets and from Taylor bubbles in gas-liquid flows. Gas entrainment can be considered beneficial or undesirable according to the situation in which it occurs. For example, jet aerators are used in a wide range of chemical processes to increase the aeration capacity. Conversely, in the manufacture production of metals the presence of gas entrainment is a problem.

The process of gas entrainment on the IS separator is similar to the process produced by inclined and vertical plunging liquid jets. The latter process is very important in industry and it has been the focus of interest for several authors since 1970 (BIN, 1993). Characteristics of this specific condition of gas entrainment, such as its mechanisms, the rate of gas entrainment and the size of the generated bubbles have been thoroughly studied. The conditions that generate gas entrainment are mostly attributed to turbulence, in which the dissipation of kinetic energy occurs. Vortices and instabilities allow the liquid phase to trap air bubbles, thus generating a two-phase air-liquid flow. Diverse methods of measurement have been used to estimate or measure the amount of gas entrained by plunging liquid jets. Beginning with photography and trapping bubbles into water-filled chambers, current studies have moved on to more advanced techniques such as high-speed filming, conductive probes and laser-based optic sensors.

Average diameter and size distribution of generated bubbles are two of the proper parameters to describe the phenomenon of gas entrainment due to a plunging jet (Van de SANDE and SMITH, 1975). In this paper, we study the gas entrainment on the IS separator as the process produced by an inclined plunging semi-circular jet. A review of the current state-of-the-art research is presented. Experimental data of average bubble diameter are compared model's predictions by Ortiz-Vidal et al. (2012).

## 3. LITERATURE REVIEW

### 3.1 Inverted-Shroud Separator

With the need for efficient gas-liquid separation upstream of centrifugal submersed pumping systems due to reasons discussed in the above section, different types of separators have been proposed by a number of authors, mostly in research directly associated with oil and gas companies. Alhanati et al. (1994) proposed a centrifugal separator, using the centrifugal force generated by a rotary mechanism to divert the liquid phase to the suction of the pump. This technique, despite offering a high EGS, works well only in the absence of Taylor bubbles and is susceptible to maintenance costs due to the presence of moving parts. A natural separator, using no additional structures other than the pipe that leads the liquid into the pump, was later proposed and modeled by Serrano (1999) and studied by authors such as Harun et al. (2003) and Marquez and Prado (2003). This separator was designed mostly for the modeling of the trajectory of bubbles upstream of the pump, in which authors reached important conclusions on the influence of working parameters such as well inclination, liquid flow and duct geometry on the final EGS. In another study, Souza et al. (2003) proposed a helical separator that aimed to eliminate the presence of moving parts. The authors used a shroud (closed-bottom pipe encasing the production pipe) with a helical structure to generate a free-surface flow that would separate the gas from the liquid through decantation. This separator, however, has a small cross-sectional area, thus limiting the maximal amount of liquid flow (i.e. production rate).

Similarly to the solution studied by Souza et al. (2003), the separator studied and modeled by Rondy et al. (1993) uses an inclined channel to reduce the velocity of liquid falling into a decantation zone surrounding a production pipe, but it relies instead on the inclination of the well itself. The authors tested this system experimentally, observing the strong influence of the liquid flow and the inclination of the system on the measured EGS. This separator was later modeled and tested by Ortiz-Vidal et al. (2012), after which Mendes (2012) performed further testing in conditions closer to the ones present in actual oil wells. The authors proposed a model for total gas separation, based on correlations that aim to predict gas entrainment inside the inner annular duct that is located between the shroud and the production pipe. This model approximates the impact between the free-surface flow generated inside the inner annular duct and the decantation zone (IAL) to a semicircular inclined plunging liquid jet.

### 3.2 Air entrainment phenomenon

Two mechanisms have been proposed to explain the air entrainment in plunging jets (see SENE, 1988). For low velocities, air enters because of disturbance of the jet, for example waves or turbulent eddies. Air entrainment occurs when forces due to dynamic pressure exceeds surface tension ones. The phenomenon is strongly dependent on the turbulence intensity of the jet. For high velocities, on the other hand, on account of the shear forces at the surface of the

jet, a continuous layer is formed and enters the liquid at a quasi-constant rate in the impact zone. The layer becomes unstable and breaks up into bubbles. Air entrainment rate is related to power 3 and 1.5 of the impact velocity (SENE, 1988).

Measurements on circular jets suggest that the transition of low-to-high speed mechanisms occurs gradually at impact velocities between 4 m/s and 10 m/s (Van de SANDE and SMITH, 1973; 1976). Based on the disruption mechanism of liquid jets, it is established that the high-speed mechanism happens at Weber number higher than 10, being defined as the ratio of air friction forces to surface tension forces (RICHARDSON, 1954; Van de SANDE and SMITH, 1976). Furthermore, air entrainment rate for low and high-speed mechanisms depend on Froude number and a combination of both Weber and Reynolds numbers, respectively.

Penetration depth is an important parameter in air entrainment phenomenon. However, a few studies have been reported. For the case of circular jets, Van de Sande and Smith (1975) state that a simple momentum approach is insufficient to determine the penetration depth. Two jets with the same diameter and velocity (same momentum) but different jet lengths will have different amount of entrained air. Then, they propose an empirical correlation which relates the four parameters: bubble penetration depth, impact velocity, jet diameter and air entrainment rate. Ortiz-Vidal *et. al* (2012) studied the air penetration depth on the IS separator due to an inclined plunging semi-circular jet (free-surface semi-circular flow), The authors suggest that the penetration depth is strongly dependent on the diameter of generated bubbles, and consequently to the energy dissipation (see Eq. (1)). For the authors, in contrast to Van de Sande and Smith (1975), the length of free-surface jet is not an important parameter. They assume that the spatial instabilities at the free-surface are negligible. Both studies are in agreement on the inclined jets are less severe that vertical ones (smaller generated bubbles), and consequently the penetration depth is lower. To compare these studies quantitatively, it is necessary to establish a link between both energy dissipation and air entrainment parameters.

Ortiz-Vidal *et. al* (2012) use Eq. 1 to predict the maximum bubble size that could exist in the air entrainment zone generated by the impact between a semi-circular jet (free-surface flow) and the receiving flow (Hinze apud GULLIVER ET AL., 1990), as happens in the IAL of the IS-separator.

$$d_b = 1.15\left(\frac{\sigma}{\rho_w}\right)^{0.6} E_{dis}^{-0.4} \tag{1}$$

where $d_{\max}$ is the maximum bubble diameter, $\sigma$ is the water-air interfacial tension, $\rho_w$ is the water specific mass and $E_{dis}$ is the energy dissipation rate per unit mass. $E_{dis}$ was considered as equal to the total dissipation of kinetic energy of the free-surface flow for simplification purposes, being then equal to

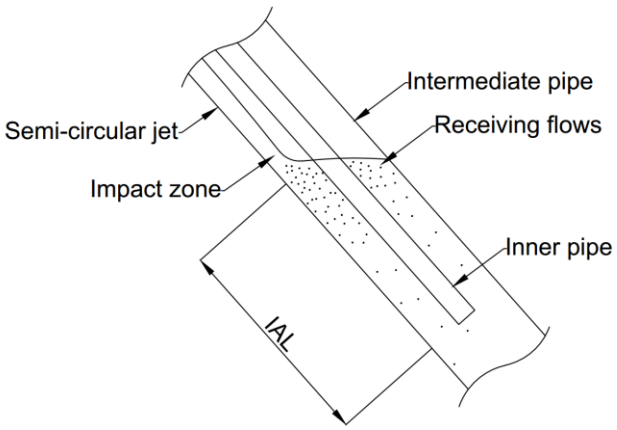


Figure 1. Bubbles generated in an IS-separator.

$$E_{dis} = \frac{1}{2}\frac{V_{fs}^2}{L_{dis}} \tag{2}$$

where $V_{fs}$ is the velocity of the free-surface flow, obtainable through known equations from the literature regarding flow in open channels, $L_{dis}$, the length of energy dissipation, is related to the water viscosity ($\mu_w$), the inclination of the channel ($\beta$) and the water flow rate ($Q_w$). Experimentally adjusted correlations were proposed by Mendes (2012) in an attempt to predict $L_{dis}$, as shown in Eqs. 3 and 4.

$$1500 D_h \left(We^*\right)^2, \text{ if } \mathrm{Re}_{fs} < 2000 \tag{3}$$

$$0.008 D_h \left(We^*\right)^2, \text{ if } \mathrm{Re}_{fs} \geq 2000 \tag{4}$$

where $D_h$ is the hydraulic diameter of the semi-circular plunging jet, $Re_{fs}$ is its Reynolds number and $We^*$ is a modified version of the Weber number, as shown in Eq. 5.

$$We^* = \frac{\rho_w S_i V_{fs}^2}{48\sigma} \tag{5}$$

where $S_i$ is the perimeter of the semi-circular jet.

### 3.3 Bubble size distribution

Evans et al. (1992) studied the size of bubbles generated by a plunging liquid jet bubble column. The authors obtained a large amount of bubble size measurements through photographic methods and were able to obtain bubble diameter distributions for varying plunging jet velocities. An average bubble size was calculated through different methods. The basis for the calculation of average particle size is Eq. 6, in which the parameters *m* and *n* can be varied for different results. Using $m = 1$ and $n = 0$, for example, would yield a diameter equivalent to the simple arithmetic average of measured diameters, or $d_{average}$.

$$d_{mn} = \left( \sum_{i=1}^{k} n_i d_i^m \Big/ \sum_{i=1}^{k} n_i d_i^n \right)^{\frac{1}{m-n}} \tag{6}$$

The Sauter average diameter $d_{Sauter}$, as proposed by Sauter (*apud* AZZOPARDI, 1979), was firstly used in the analysis of droplet size in carburetors. The author uses $m = 3$ and $n = 2$, resulting in an average size that is mostly dependent on the particle's volume and superficial area. These characteristics are generally considered important in the study of bubble formation and breakage and therefore can be used to evaluate bubble size distributions. Evans et al. (1992) compared the average Sauter diameter of the obtained distributions with the maximum bubble diameter $d_{\max}$, which is defined as the diameter that is bigger than 99% of all measured diameters in the distribution. The authors have found that the ratio $d_{Sauter}/d_{\max}$ remains approximately the same for all measured distributions, being equal to 0.61. This is in accordance with the literature, where other studies (ZHANG et al., 1985; CALABRESE et al., 1986) have found this measure to be in the range of 0.60 to 0.62.

## 4. EXPERIMENTAL WORK

### 4.1 Test Loop

Experiments were conducted at the Thermal-Fluids Engineering Laboratory (LETeF) of the Mechanical Engineering Department of the Engineering School of Sao Carlos, University of Sao Paulo (USP). The experimental apparatus used in this work is made of a test section, measurement systems and air/water supply systems. A diagram of the apparatus and a list of its components can be seen in Fig. 2 and Tab. 1, respectively. The test section is an IS-separator composed of PVC and borosilicate glass tubing installed concentrically, as shown in Fig. 2. The internal and external diameters of the inner annular duct (between the intermediate pipe and the inner pipe, as described in Fig. 1) are equal to 32 mm and 53 mm, respectively. A 155-mm diameter pipe concentric to the annular duct is used to isolate and pressurize the system, working in the same manner as the well casing. This allows for the maintenance of a steady-state flow in which the level of liquid inside the annular duct can be controlled through the liquid flowrate and the pressure inside the system. The test section is supported by a steel structure that can be inclined at any angle between 0-90º.

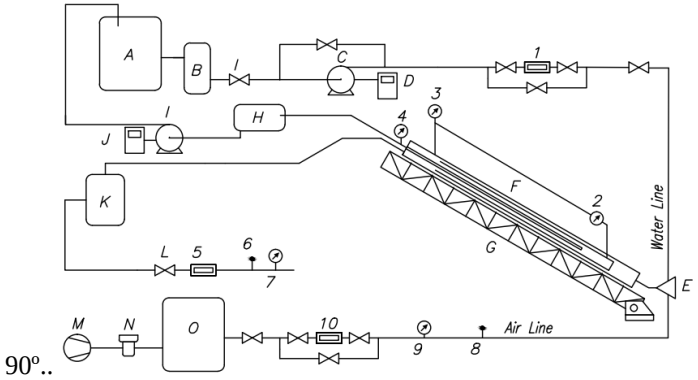


Figure 2. Experimental test loop.

Table 1. Components of the test loop.

| Letter | Component |
|---|---|
| A | Oil/water separator |
| B | Water reservoir |
| C | Screw pump |
| D | Frequency shifter |
| E | Air-water mixer |
| F | Test section |
| G | Inclinable structure |
| H | Water reservoir |
| I | Screw pump |
| J | Frequency shifter |
| K | Air/water separator |
| L | Pressure control valve |
| M | Air compressor |
| N | Air filter system |
| O | Air tank |

Table 2. Measurements instruments of the test loop

| Number | Component | Manufacturer/Model | Range | Accuracy |
|---|---|---|---|---|
| 1 | Water flowmeter | Oval EX Delta | 30- 1300 (l/min) | 1% RD |
| 2 | Differential pressure transmitter | Smar LD 301 | 1- 50 (kPa) | 0.075% Span |
| 3 | Pressure transmitter | Huba Control 510 | 0- 5 (bar) | 0.25% FE |
| 4 | Pressure transmitter | Huba Control 961 | -1-1 (bar) | 0.3% FE |
| 5 | Air flowmeter | Contech SVTG ½'' | 1.37- 13.7 (m³/h) | 1% FE |
| 6 | Mercury thermometer | Princo 453 | 15- 50 (ºC) | 0.5 ºC |
| 7 | Mercury barometer | Princo 453 | 647-830 (mmHg) | 0.5 mmHg |
| 8 | Temperature transmitter | IOPE TW-TC/2 | -20- 140 (ºC) | 0.5 ºC |
| 9 | Pressure transmitter | Danfoss AKS 33 | 0-1 (bar) | 0.8% FE |
| 10 | Air flowmeter | Oval GAL 50 | 1- 20 (l/min) | 1% FE |

Water and air were supplied with the use of a Weatherford 2WHT53 screw pump and a Schulz SRP-3030 compressor, respectively. Measurement instruments are shown in Tab. 2. Water flowrate was measured with the use of positive displacement flowmeter (1). Air mass flow was measured at the inlet of the test loop with a volumetric flowmeter (10), a thermocouple (8) and a pressure transducer (9). In the same way, air mass flow was also measured at the outlet of the test loop with sensors 5, 6 and 7. Air temperature and pressure on the outlet of the test loop were assumed to be the same as the atmospheric conditions.

Air and water were injected with the use of a mixer (E) through the bottom of the outer annular duct. An air outlet, located at the upper end of the outer annular duct, collects gas that was not entrained in the water phase. The test loop's equipment (pumps and valves) are controlled with the use of an in-house developed LabVIEW-based interface, coupled with a National Instruments PXI data acquisition board.

### 4.2 Optical Reflectance Measurement (ORM)

Bubble size measurements were performed with the use of the three-dimensional Optical Reflectance Measurement (3D ORM) technique. Lovick et al. (2005) reported good results with this type of measurement technique in comparison with data acquired with a high-speed camera coupled with an endoscope, with which droplet sizes were acquired in an oil-water agitated mixture. In the present work this was similarly performed with an ORM IDAS (In situ Droplet Aerosol Analysis System based on ORM with spiral vertical moving selective focus), provided by SEQUIP™. The apparatus provides *in-situ* and on-line bubble and drop size measurements through the use of a 1-5mW laser beam coupled with lenses that allow its focal point to be rapidly adjusted in front of it. The focal point is rotated at a fixed rate, making it possible to track 3D volumes of bubbles with diameters ranging from 1 to 3000 µm. The chord length of bubbles and droplets scatters the beam of the laser, sending light back into a detector inside the probe that transforms it into an electrical signal that can be then converted analytically into a diameter, assuming the particles are spherical. This conversion is made automatically with software provided by SEQUIP™, WinORM 5.1, which can also be used for basic analysis of the acquired particle size distributions.

A probe surrounds the measurement equipment, allowing it to be installed *in situ*, solving problems associated with filming such as light source power and positioning. The 3D ORM probe was installed at a distance of 7,5m from the inlet of the annular duct with a perforated PVC sleeve, as shown in Fig. 3. The probe was installed at an angle of 15º in relation to the central axis of the apparatus, as oriented by SEQUIP™. Data was acquired during steady-state flow in which the inner annular level (IAL) was controlled and measured with the use of differential pressure transducers. The distance between the impact zone and the probe window, $L_{window}$, therefore, could also be measured.

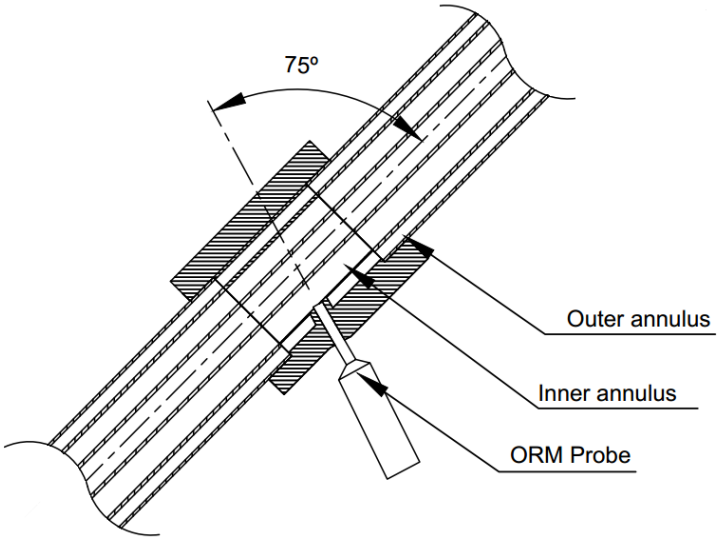


Figure 3. ORM probe installation.

### 4.3 ORM Probe Validation

The 3D ORM system was validated with the aid of spherical hollow glass microspheres, commonly used with Particle Image Velocimetry (PIV) systems, with average diameters ranging from 8 to 11 µm according to the manufacturer. The microspheres were dispersed in distilled water in a 1000 ml beaker, with aid from a magnetic mixer. The ORM probe was inserted into the beaker, both before and after the insertion of the microspheres, and in both cases particle size distribution measurements were made. Fig. 4 shows histograms obtained with the WinORM software. The distribution of particles of water before adding the microspheres was discounted from the sample collected after the addition, to eliminate noise. The measured average diameter $d_{average}$ equals 13 µm, which is in fair accordance with expected results.

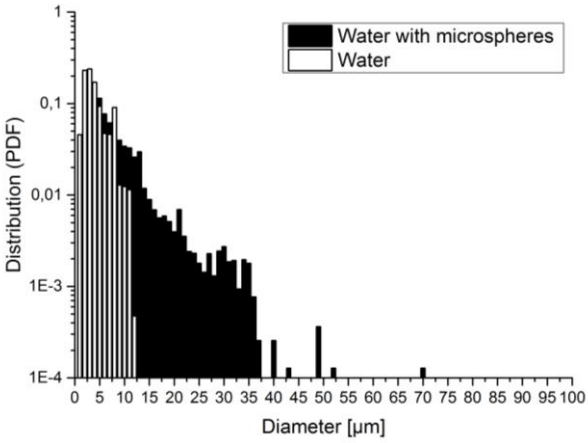


Figure 4. ORM probe validation results.

### 4.4 Experimental Procedure

The experimental procedure begins with the adjustment of the inclination angle of the test section, after which the air compressor and pump were started. After the compressed-air supply tank reaches the pressure of 7.5 barg, the air and water injection valves were opened and the flow rates were set. The IAL position was then adjusted by opening or closing the air pressure regulation valve on the air outlet of the test section, while the internal pressure was read through the LabVIEW interface. After steady-state flow was reached, condition monitored by the differential-pressure-transducer readings (2, Fig. 2) that would display a constant value, data acquisition could then be initiated both on the LabVIEW interface and on WinORM. When the acquisition period is completed, this procedure was repeated for other IAL positions.

## 5. RESULTS

Data was acquired at a constant volumetric water flow rate of approximately $Q_w$ = 60 l/min and with the test section inclined at $\beta$ = 45º. The internal pressure inside the outer casing was controlled to allow for bubble diameter distribution measurements at three different IAL positions, as shown in Tab. 3. Through this variation, the authors expected to obtain the characteristic length related to the free-surface-flow kinetic-energy dissipation, namely $L_{dis}$. The obtaining of $L_{dis}$ is based on the following three hypotheses. (i) Near the impact zone the entrained bubbles are still large, since the breaking up process due to turbulence requires some development length, (ii) Hinze's maximum bubble diameter $d_{\max}$ is established at the point that the development length of the breaking-up process is reached, and (iii) after $L_{dis}$ the number of bubbles in the distribution start to decrease due to buoyancy effects.

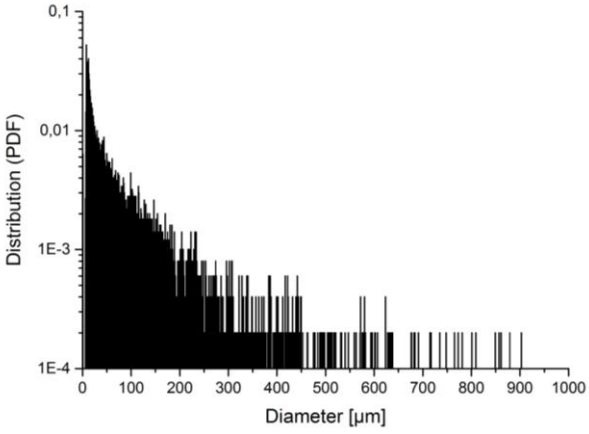


Figure 5: Bubble size distribution acquired with $L_{probe}$ = 2.70 m.

Table 3. Experimental results.

| Test | $L_{probe}$ [m] | $d_{average}$ [μm] | $d_{Sauter}$ [μm] | $d_{\max}$ [μm] | $\frac{d_{Sauter}}{d_{\max}}$ |
|---|---|---|---|---|---|
| 01 | 2.92 | 70.43 | 382.37 | 471 | 0.81 |
| 02 | 2.70 | 75.92 | 399.55 | 512 | 0.78 |
| 03 | 1.43 | 64.70 | 349.23 | 476 | 0.73 |

Bubble size distributions were acquired through the use of the ORM probe. One example of an acquired distribution can be seen in Fig. 5. According to the phenomenological model proposed by Ortiz-Vidal et al. (2012) and improved by Mendes (2012), the expected maximum bubble size equals 58 μm. Experimental results, (Tab. 3 and Fig. 6), however, show a significant difference from the expected value, possibly indicating that Ortiz-Vidal's model must be further adjusted. The small amount of data sets obtained, however, did not make it possible to characterize a decrease in bubble size as $L_{\text{probe}}$ increases. More experiments need to be conducted.

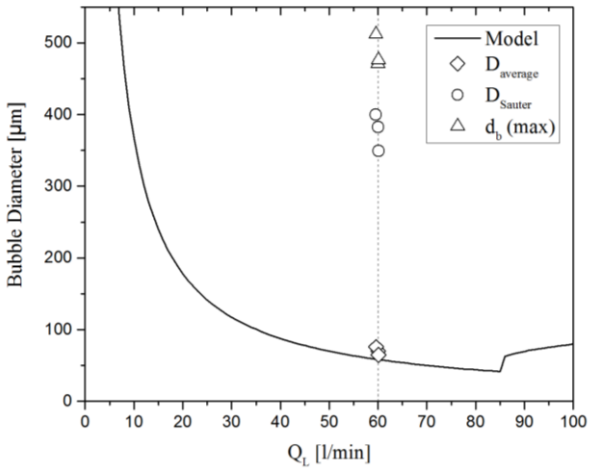


Figure 6. Results from Tab. 3 in comparison to the phenomenological model.

The obtained ratio between the Sauter diameter and the maximum diameter was, on average, similar to that measured by Evans et al. (1992). Some disagreement was expected, since in that work they studied the size of bubbles generated by a plunging liquid jet bubble column, which is different from the case studied in the present work.

## 6. ACKNOWLEDGEMENTS

The authors thank the support of The Brazilian National Council for Scientific and Technological Development (CNPq, contracts 164211/2015-2, 501443/2014-2 and 151317/2014-3), PETROBRAS, and the National Petroleum Agency (ANP).

## 7. REFERENCES

Alhanati, F.J.S., Sambangi, S.R., Doty, D.R., Schmidt, Z., 1994. A Simple Model for the Efficiency of Rotary Separators, in: Proceedings of SPE Annual Technical Conference and Exhibition. Society of Petroleum Engineers, New Orleans, LA, USA, pp. 67-82. Doi: 10.2118/28525-MS.

Azzopardi, B.J., 1979. "Measurement of Drop Sizes", International Journal of Heat and Mass Transfer, Vol. 22, No. 9, pp. 1245-1279.

Bin, A., 1993. "Gas Entrainment by Plunging Jets", Chemical Engineering Science, Vol. 48, No. 21, pp. 3385-3630.

Barbosa, M.C., 2015. Investigação da Distribuição de Tamanho de Bolhas em um Separador Gás-Líquido do Tipo Shroud Invertido. Universidade de São Paulo, Escola de Engenharia de São Carlos, São Carlos, SP, Brazil.

Calabrese, R.V., Chang T.P.K. and Dang P.T., 1986. "Drop Breakup in Turbulent Stirred-Tank Contactors, Part I: Effect of Dispersed-Phase Viscosity", A.I.C.h.E. Journal, Vol. 32, pp. 657-666.

Evans, G.M., Jameson, G.J. and Atkinson, B.W., 1992. "Prediction of The Bubble Size Generated by a Plunging Liquid Jet Bubble Column", Chemical Engineering Science, Vol. 47, pp. 3265-3272.

Gulliver, J.S., Thene, J.R. and Rindels, A.J., 1990. "Indexing Gas Transfer in self-aerated flows", Journal of Environmental Engineering, Vol. 116, pp. 503-523.

Lovick, J., Mouza, A.A., Paras, S.V., Lye G.J. and Angeli, P., 2005. "Drop Size Distribution in Highly Concentrated Liquid-Liquid Dispersions Using a Light Back Scattering Method", Journal of Chemical Technology and Biotechnology, Vol. 80, pp. 545-552.

Mendes, F.A.A., 2012. Estudo Experimental, Simulação Numérica e Modelagem Fenomenológica da Separação Gravitacional de Gás no Fundo de Poços Direcionais. Ph.D. thesis, University of Sao Paulo, Sao Carlos, SP, Brazil.

Ortiz-Vidal, L.E., 2011. Separação gravitacional de gás em um duto anular inclinado: estudo experimental e modelagem fenomenológica. Universidade de São Paulo, Escola de Engenharia de São Carlos, São Carlos, SP, Brazil

Ortiz-Vidal, L.E., Rodriguez, O.M.H, Estevam, V. and Lopes, D., 2012. "Experimental Investigation of Gravitational Gas Separation in an Inclined Annular Channel", Experimental Thermal and Fluid Science, Vol. 39, pp. 17-25.

Richardson, E. G., 1954. "Mechanism of the Disruption of Liquid Jets", Applied Scientific Research, Section A, 4(5-6), pp. 374–380.

Sene, K.J., 1988. "Air Entrainment by Plunging Jets", Chemical Engineering Science, Vol. 43, pp. 2615-2623.

Serrano, J.C., 1999. Natural separation efficiency in electric submersible pump systems. MSc thesis, University of Tulsa, Tulsa, OK, USA.

Souza, R. de O., Lopes, D., Cosa, R. de O., Estevam, V., 2003. Separador de gás de fundo de poço de alta eficiência, in: Seminario de Elevação Artificial, Escoamento e Medição. PETROBRÁS - Petróleo Brasileiro S.A., Rio de Janeiro, Brasil.

Van de Sande, E., and Smith, J., 1973. "Surface Entrainment of Air by High Velocity Water Jets", Chemical Engineering Science, pp. 1161–1168.

Van De Sande, E., and Smith, J. M., 1976. "Jet Break-Up and Air Entrainment by Low Velocity Turbulent Water Jets", Chemical Engineering Science, Vol. 31(3), pp. 219–224.

Van de Sande, E., and Smith, J. M., 1975. "Mass Transfer From Plunging Water Jets", The Chemical Engineering Journal, Vol. 10(3), pp. 225–233.

Zhang S.H., Yu, S.C., Zhou Y.C. and Su Y.F., 1985. "A Model for Liquid-Liquid Extraction Column Performance – The Influence of Drop Size Distribution on Extraction Efficiency", The Canadian Journal of Chemical Engineering, Vol. 63, pp. 212-226.

## 7. RESPONSIBILITY NOTICE

The authors are the only responsible for the printed material included in this paper.